
Log Gaussian Cox Process Networks

Virginia Aglietti
University of Warwick
V.Aglietti@warwick.ac.uk

Theo Damoulas
University of Warwick
T.Damoulas@warwick.ac.uk

Edwin Bonilla
The University of New South Wales
e.bonilla@unsw.edu.au

Abstract

We generalize the log Gaussian Cox process (LGCP) framework to model multiple correlated point data jointly. The resulting log Gaussian Cox process network (LGCPN) considers the observations as realizations of multiple LGCPs, whose log intensities are given by linear combinations of latent functions drawn from Gaussian process priors. The coefficients of these linear combinations are also drawn from Gaussian processes and can incorporate additional dependencies a priori. We derive closed-form expressions for the moments of the intensity functions in our model and use them to develop an efficient variational inference algorithm that is orders of magnitude faster than competing deterministic and stochastic approximations of multivariate LGCP and coregionalization models. Our approach outperforms the state of the art in jointly estimating multiple bovine tuberculosis incidents in Cornwall, UK, and multiple crime type intensities across New York city.

1 Introduction

Many problems in urban science and computational sustainability [10] are characterized by count or point data observed in a spatio-temporal region. Species observations in ecological applications, events that unfold in our cities, crime or other social activities, traffic and human population dynamics are some examples. Furthermore, in many settings these processes do not occur in isolation but can be strongly correlated. For example, in a city such as New York (NYC), burglaries in different regions can be highly predictive of other crimes' occurrences such as robberies and larcenies. We refer to these settings as multi-task problems and our goal is to exploit such dependencies in order to improve the generalization capabilities of our learning algorithms.

These problems can be modeled as inhomogeneous processes where a space-time varying underlying intensity determines event occurrences. Among these modeling approaches, the log Gaussian Cox process [LGCP, 19] is one of the most well-established frameworks, where the intensity is driven by a Gaussian process prior [GP, 28]. The flexibility of these models comes at the cost of incredibly hard inference challenges, which are a consequence of the doubly-stochastic nature of LGCPs and the notorious scalability issues of GP models. These computational problems are exacerbated when considering multiple correlated modalities and, therefore, the development of new approaches and scalable inference algorithms for LGCP models remains an active area of research [8, 9, 14, 24].

From a modeling perspective, most current approaches can be seen as being multivariate LGCPs where the intensities are *deterministic* combinations of latent GPs [3, 8, 12, 24]. These modeling frameworks do not propagate uncertainty in the weights of the linear combination and may overfit when the weights are deterministic, see Fig. 1. From an inference point of view, sampling approaches have been proposed before [8, 24] and variational inference algorithms for models with GP priors and

‘black-box’ likelihoods can (and indeed have) been used [see e.g. 7, 18]. While sampling approaches have been shown to have critical mixing issues, generic methods based on variational inference, by definition, do not exploit the details of the likelihood and can exhibit slow convergence, as they rely upon Monte Carlo estimates for computing the required expectations during optimization.

Contribution In this paper we propose to jointly model correlated count data as realizations of multiple LGCPs, where the log intensities are linear combinations of latent GP. Unlike previous work, the coefficients of these linear combinations are also drawn from GPs. This allows us to incorporate additional task dependencies providing better uncertainty quantification. Despite the additional flexibility, we derive closed-form expressions for the moments of the intensity functions which allows us to develop an efficient variational approximation. We offer the state of the art on two large datasets in terms of prediction accuracy while being orders of magnitude faster than competing deterministic and stochastic approximations of multivariate LGCP and coregionalization models. Because our method can be seen as a generalization of the existing multi-task LGCP frameworks characterized by an underlying network of intensities, we term it log Gaussian Cox process networks (LGCPN).

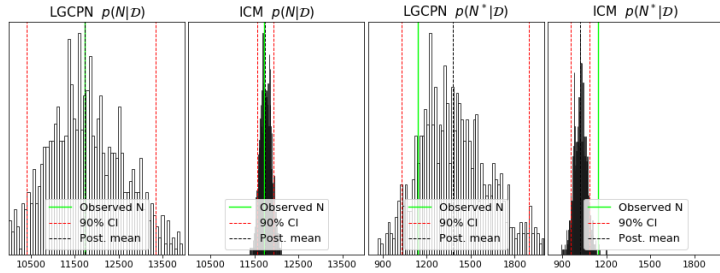


Figure 1: Posterior and predictive distributions, $p(N|\mathcal{D})$ and $p(N^*|\mathcal{D})$ respectively, of the number of burglary events in NYC using a similar analysis as in [14] on the CRIME dataset (§5.2) for our model (LGCPN) and the intrinsic coregionalization model (ICM). The solid line shows the ground truth.

2 Log Gaussian Cox process networks

The log Gaussian Cox process [LGCP, 19] is an inhomogeneous Poisson process with a stochastic intensity function [see e.g. 5], where the logarithm of the intensity surface is a GP [28]. Given an input \mathbf{x} , a GP, denoted as $f(\mathbf{x}) \sim \mathcal{GP}(m(\mathbf{x}), \kappa(\mathbf{x}, \mathbf{x}'; \boldsymbol{\theta}))$, is completely specified by its mean function $m(\mathbf{x})$ and its covariance function $\kappa(\mathbf{x}, \mathbf{x}'; \boldsymbol{\theta})$ parametrized by the hyper-parameters $\boldsymbol{\theta}$. Conditioned on the realization of the intensity function, the number of points in an area, say A , is given by $y_A | \lambda(\mathbf{x}) \sim \text{Poisson}(\int_{\mathbf{x} \in A} \lambda(\mathbf{x}) d\mathbf{x})$ with $\lambda(\mathbf{x}) = \exp\{f(\mathbf{x})\}$. Consider a dataset $\mathcal{D} = \{(\mathbf{x}_n, y_n)\}_{n=1}^N$, where \mathbf{x}_n is a D -dimensional vector denoting the centroid of the n -th cell on a regular computational grid and y_n is the number of events in that cell. For each n , the LGCP observation model can be written as $y_n | f(\mathbf{x}_n) \sim \text{Poisson}(\exp[f(\mathbf{x}_n) + m])$ where m is an offset to the log-mean of the process.

2.1 Model formulation

LGCPN is characterized by Q latent functions which are uncorrelated a priori and are drawn from Q zero-mean GPs, i.e. $f_q | \boldsymbol{\theta}_q \sim \mathcal{GP}(\mathbf{0}, \kappa(\mathbf{x}, \mathbf{x}'; \boldsymbol{\theta}_q))$, for $q = 1, \dots, Q$. Hence, the prior over all the $N \times Q$ latent function values \mathbf{F} is:

$$p(\mathbf{F} | \boldsymbol{\theta}) = \prod_{q=1}^Q p(\mathbf{F}_{\bullet q} | \boldsymbol{\theta}_q) = \prod_{q=1}^Q \mathcal{N}(\mathbf{F}_{\bullet q}; \mathbf{0}, \mathbf{K}_{xx}^q), \quad (1)$$

where $\boldsymbol{\theta}_q$ is the set of hyper-parameters for the q -th latent function and $\mathbf{F}_{\bullet q} = \{f_q(\mathbf{x}_n)\}_{n=1}^N$ denotes the values of latent function q for the observations $\mathbf{x}_1, \dots, \mathbf{x}_N$. We model correlation among the tasks by linearly combining the above latent functions with a set of task-specific mixing weights, $\mathbf{W} \in \mathbb{R}^{P \times Q}$, which determine the contribution of each latent function to the overall LGCP intensity. We consider two possible prior distributions for \mathbf{W} , an independent prior and a correlated prior.

Prior over weights We assume weights drawn from Q zero-mean GPs:

$$p(\mathbf{W}|\boldsymbol{\theta}_w) = \prod_{q=1}^Q \mathcal{N}(\mathbf{W}_{\bullet q}; \mathbf{0}, \mathbf{K}_w^q), \quad (2)$$

where $\mathbf{W}_{\bullet q}$ represents the P weights for the q -th latent function and $\boldsymbol{\theta}_w$ denotes the hyper-parameters. In the independent scenario, we assume uncorrelated weights across tasks and latent functions by making \mathbf{K}_w^q diagonal. Note that, despite considering uncorrelated weights, the observations across tasks will still be correlated via the linear mixing of latent random functions.

Likelihood model Following a common approach (see the supplementary material) we introduce a computational grid [8] on the spatial extent and represent each cell with its centroid. Under LGCPN, the likelihood of the observations is defined for each task as a LGCP with a log intensity given by the linear combination of the latent functions. Therefore, assuming i.i.d. observations, we have that:

$$p(\mathbf{Y}|\mathbf{F}, \mathbf{W}) = \prod_{n=1}^N \prod_{p=1}^P \text{Poisson}(y_{np}; \exp(\mathbf{W}_{p\bullet} \mathbf{F}_{n\bullet} + \phi_p)), \quad (3)$$

where $\mathbf{W}_{p\bullet}$ represents the Q weights for the p -th task, $\mathbf{F}_{n\bullet}$ denotes the Q latent function values corresponding to observation n , and ϕ_p indicates the task-specific offset to the log-mean of the Poisson process.

As in the standard LGCP model, the introduction of a GP prior poses significant computational challenges during posterior estimation as, naïvely, inference would be dominated by algebraic operations that are cubic on N . In order to make inference scalable, we follow the inducing-variable approach proposed by [25] and further developed by [4]. To this end, we augment our prior over the latent functions in Eq. (1) with M underlying *inducing variables* for each latent process. We denote these M inducing variables for latent process q with $\mathbf{U}_{\bullet q}$ and their corresponding *inducing inputs* with the $M \times D$ matrix \mathbf{Z}_q . We will see that major computational gains are realized when $M \ll N$. Hence, we have that the prior distributions for the inducing variables and the latent functions can be written as:

$$p(\mathbf{U}|\boldsymbol{\theta}) = \prod_{q=1}^Q \mathcal{N}(\mathbf{U}_{\bullet q}; \mathbf{0}, \mathbf{K}_{zz}^q) \quad (4) \quad p(\mathbf{F}|\mathbf{U}, \boldsymbol{\theta}) = \prod_{q=1}^Q \mathcal{N}(\mathbf{F}_{\bullet q}; \tilde{\boldsymbol{\mu}}_q, \tilde{\mathbf{K}}^q), \quad (5)$$

where the conditional prior mean $\tilde{\boldsymbol{\mu}}_q = \mathbf{K}_{xz}^q (\mathbf{K}_{zz}^q)^{-1} \mathbf{U}_{\bullet q}$ and the covariance $\tilde{\mathbf{K}}^q = \mathbf{K}_{xx}^q - \mathbf{K}_{xz}^q (\mathbf{K}_{zz}^q)^{-1} \mathbf{K}_{zx}^q$. \mathbf{U} is the set of all the inducing variables; the matrices \mathbf{K}_{xx}^q , \mathbf{K}_{xz}^q , \mathbf{K}_{zx}^q and \mathbf{K}_{zz}^q are the covariances induced by evaluating the corresponding covariance functions at all pairwise rows of the training inputs \mathbf{X} and the inducing inputs \mathbf{Z}_q ; and $\boldsymbol{\theta} = \{\boldsymbol{\theta}_q\}_{q=1}^Q$ represents the set of hyper-parameters for the Q latent functions. Notice that by integrating out \mathbf{U} from the augmented prior distribution in Eqs. (4) and (5) we can recover the initial prior distribution in Eq. (1) exactly.

2.2 Closed-form moment generating function of log intensities

LGCPN allows to compute the moments of $\boldsymbol{\lambda}$ in closed form. The t -th moment for the p -th task intensity evaluated at \mathbf{x}_n , namely $\mathbb{E}[\lambda_p(\mathbf{x}_n)^t]$, can be written as $\exp(t\phi_p) \mathbb{E}[\exp(t\mathbf{W}_{p\bullet} \mathbf{F}_{n\bullet})] = \exp(t\phi_p) \text{MGF}_{\mathbf{W}_{p\bullet} \mathbf{F}_{n\bullet}}(t)$ where $\text{MGF}_{\mathbf{W}_{p\bullet} \mathbf{F}_{n\bullet}}(t)$ denotes the moment generating function of $\mathbf{W}_{p\bullet} \mathbf{F}_{n\bullet}$ evaluated in t . As the random variable resulting from $\mathbf{W}_{p\bullet} \mathbf{F}_{n\bullet}$ is the sum of products of independent Gaussians, its MGF can be written as [6]:

$$\text{MGF}_{\mathbf{W}_{p\bullet} \mathbf{F}_{n\bullet}}(t) = \prod_{q=1}^Q \frac{\exp\left[\frac{t\gamma_{pq}\tilde{\mu}_{nq} + 1/2(\tilde{\mu}_{nq}^2 K_w^q(p) + \gamma_{pq}^2 \tilde{K}^q(n))t^2}{1 - t^2 K_w^q(p) \tilde{K}^q(n)}\right]}{\sqrt{1 - t^2 K_w^q(p) \tilde{K}^q(n)}}, \quad (6)$$

where the expectation is computed with respect to the prior distribution of $\mathbf{W}_{p\bullet}$ and $\mathbf{F}_{n\bullet}$; γ_{pq} is the prior mean of w_{pq} ; $\tilde{K}^q(n)$ denotes the variance of f_{nq} ; and $K_w^q(p)$ is the variance of w_{pq} . We can now use the expression in Eq. (6) to show that our approach can be seen as a generalization of previous methods for modeling count data.

LEMMA 1 LGCPN generalizes ICM, MLGCP and LGCP. As $\mathbf{K}_w \rightarrow 0$, for $Q \neq P$ we have $\hat{\lambda}_{\text{LGCPN}} \rightarrow \hat{\lambda}_{\text{ICM}}$ (or a $\hat{\lambda}_{\text{LGCPN}} \rightarrow \hat{\lambda}_{\text{LCM}}$ depending on the assumed covariance functions for the latent GPs) where the intensity parameters are jointly determined by the moments of \mathbf{F} and \mathbf{W} :

$$\lim_{\mathbf{K}_w \rightarrow 0} \text{Cov}(\log \lambda_p(\mathbf{x}), \log \lambda_{p'}(\mathbf{x}')) = \sum_{q=1}^Q \underbrace{\gamma_{pq} \gamma_{p'q'}}_{\mathbf{B}^{q(p,p')}} \tilde{\mathbf{K}}_{\mathbf{xx}'}^q \quad (7)$$

where $\mathbf{B}_q \in \mathbb{R}^{P \times P}$ is known as coregionalisation matrix. For $Q = P + 1$ and $\mathbf{W}_{P \times (P+1)} = [\mathbf{I}_P \ \mathbf{1}_P]$ we have $\hat{\lambda}_{\text{LGCPN}} \rightarrow \hat{\lambda}_{\text{MLGCP}}$. Finally, for $Q = P$ and $\mathbf{W}_{P \times P} = \mathbf{I}_P$ we have $\hat{\lambda}_{\text{LGCPN}} \rightarrow \hat{\lambda}_{\text{LGCP}}$.

The details of derivations of Eqs. (6) and lemma 1 are in the supplement but the theoretical and practical consequences are worth highlighting. Despite our LGCPN being a more flexible approach to modeling correlated count data than previous methods, we can still compute its moments in closed form. Furthermore, by assuming a posterior over weights and functions structurally analogous to the prior, we will be able to compute the required expectations of the conditional likelihood required during variational inference in closed form and avoid Monte Carlo estimates altogether. We will show the details of this in the next section.

3 Inference

Given the prior distributions over the weights in Eq. (2); the joint prior over the latent functions and inducing variables in Eqs. (4) and (5); and the likelihood model in Eq. (3), our goal is to estimate the posterior over all latent variables given the observed data, i.e. $p(\mathbf{F}, \mathbf{U}, \mathbf{W} | \mathcal{D})$. This posterior is analytically intractable and we resort to variational inference [13]. Variational inference methods aim to minimize the Kullback-Leiber (KL) divergence between the joint approximated posterior and the true joint posterior. This is equivalent to maximizing the so-called evidence lower bound, $\mathcal{L}_{\text{elbo}}$.

3.1 Variational Distributions

We define our variational distribution as $q(\mathbf{F}, \mathbf{U}, \mathbf{W} | \boldsymbol{\nu}) = p(\mathbf{F} | \mathbf{U})q(\mathbf{U} | \boldsymbol{\nu}_u)q(\mathbf{W} | \boldsymbol{\nu}_w)$ where $\boldsymbol{\nu}$ denotes variational parameters. The choice for this variational distribution, in particular with regards to the incorporation of the conditional prior $p(\mathbf{F} | \mathbf{U})$, is motivated by the work of Titsias [25], and will yield a decomposition of the evidence lower bound and ultimately will allow scalability to very large datasets through stochastic optimization. We define the variational distribution for \mathbf{U} and \mathbf{W} as:

$$q(\mathbf{U} | \boldsymbol{\nu}_u) = \prod_{q=1}^Q \mathcal{N}(\mathbf{U}_{\bullet q}; \mathbf{m}_q, \mathbf{S}_q) \quad (8) \quad q(\mathbf{W} | \boldsymbol{\nu}_w) = \prod_{q=1}^Q \mathcal{N}(\mathbf{W}_{\bullet q}; \boldsymbol{\omega}_q, \boldsymbol{\Omega}_q) \quad (9)$$

where $\boldsymbol{\nu}_u = \{\mathbf{m}_q, \mathbf{S}_q\}$ and $\boldsymbol{\nu}_w = \{\boldsymbol{\omega}_q, \boldsymbol{\Omega}_q\}$ are the variational parameters. When considering an uncorrelated prior over the weights, we assume an uncorrelated posterior by forcing $\boldsymbol{\Omega}_q$ to be diagonal. Eqs. (8) and (9) fully define our approximate posterior. With these, we give details of the variational objective function, i.e. $\mathcal{L}_{\text{elbo}}$, we aim to maximize with respect to $\boldsymbol{\nu}_u$ and $\boldsymbol{\nu}_w$.

3.2 Evidence Lower Bound

Following standard variational inference arguments, it is straightforward to show that $\mathcal{L}_{\text{elbo}}$ decomposes as the sum of a KL-divergence term (\mathcal{L}_{kl}) between the approximate posterior and the prior, and an expected log likelihood term (\mathcal{L}_{ell}), where the expectation is taken over the approximate posterior. We can write $\mathcal{L}_{\text{elbo}}(\boldsymbol{\nu}) = \mathcal{L}_{\text{kl}}(\boldsymbol{\nu}) + \mathcal{L}_{\text{ell}}(\boldsymbol{\nu})$ where $\mathcal{L}_{\text{kl}}(\boldsymbol{\nu}) = -\text{KL}(q(\mathbf{F}, \mathbf{U}, \mathbf{W} | \boldsymbol{\nu}) || p(\mathbf{F}, \mathbf{U}, \mathbf{W}))$ and $\mathcal{L}_{\text{ell}}(\boldsymbol{\nu}) = \mathbb{E}_{q(\mathbf{F}, \mathbf{U}, \mathbf{W} | \boldsymbol{\nu})} [\log p(\mathbf{Y} | \mathbf{F}, \mathbf{W})]$.

KL-Divergence Term The definition of the variational distribution as $p(\mathbf{F} | \mathbf{U})q(\mathbf{U} | \boldsymbol{\nu}_u)q(\mathbf{W} | \boldsymbol{\nu}_w)$ significantly simplifies the computation of \mathcal{L}_{kl} , where the terms containing the latent functions \mathbf{F} vanish, yielding $\mathcal{L}_{\text{kl}}(\boldsymbol{\nu}) = \mathcal{L}_{\text{ent}}^u(\boldsymbol{\nu}_u) + \mathcal{L}_{\text{cross}}^u(\boldsymbol{\nu}_u) + \mathcal{L}_{\text{ent}}^w(\boldsymbol{\nu}_w) + \mathcal{L}_{\text{cross}}^w(\boldsymbol{\nu}_w)$. The expressions and the full derivations for each of these terms are given in the supplementary material.

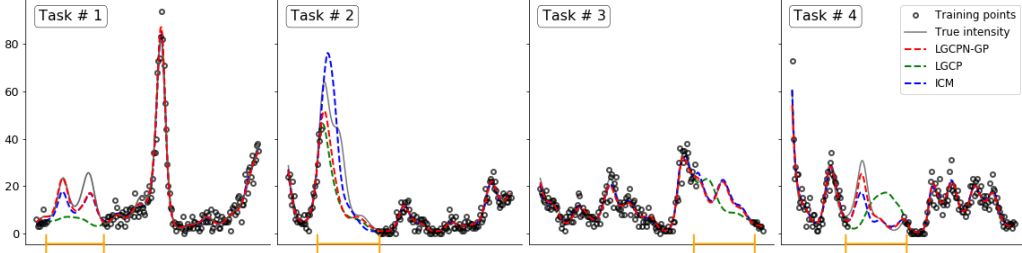


Figure 2: Four related tasks evaluated at 200 evenly spaced points in $[-1.5, 1.5]$. $|-|$ denote the 50 contiguous observations removed from the training set of each task.

3.3 Closed-form Expected Log Likelihood Term

Despite the additional model complexity introduced by the stochastic nature of the mixing weights, the expected log-likelihood term \mathcal{L}_{ell} can be evaluated in closed form:

$$\mathcal{L}_{\text{ell}}(\nu) = - \sum_{n=1}^N \sum_{p=1}^P \underbrace{\mathbb{E}_{q(\mathbf{F}_{n\bullet})q(\mathbf{W}_{p\bullet})} (\exp(\mathbf{W}_{p\bullet} \mathbf{F}_{n\bullet}))}_{\text{MGF}_{\mathbf{W}_{p\bullet} \mathbf{F}_{n\bullet}}(1)} + \sum_{n=1}^N \sum_{p=1}^P \sum_{q=1}^Q [y_{np}(\omega_{pq}\mu_{nq} + \phi_p) - \log(y_{np}!)]$$

where μ_{nq} is the mean of the variational posterior over the latent function F_{nq} , which can be obtained analytically by marginalizing \mathbf{U} from our joint variational distribution. The term $\text{MGF}_{\mathbf{W}_{p\bullet} \mathbf{F}_{n\bullet}}(1)$ is computed evaluating Eq. (6) at $t = 1$ given the current variational parameters for $q(\mathbf{W})$ and $q(\mathbf{F})$. Evaluating \mathcal{L}_{ell} in closed form allows to significantly speed up the algorithm achieving similar performance but 2 times faster on the CRIME dataset (§5.2, see Fig. (2) and Fig. (3) in the appendix).

Algorithm complexity and implementation The time complexity of our algorithm is dominated by algebraic operations on \mathbf{K}_{zz}^q , which are $\mathcal{O}(M^3)$, while the space complexity is dominated by storing \mathbf{K}_{zz}^q , which is $\mathcal{O}(M^2)$ where M denotes the number of inducing variables per latent process. \mathcal{L}_{ent} and $\mathcal{L}_{\text{cross}}$ only depends on distributions over M dimensional variables. Their computational complexity is independent of N . In addition, \mathcal{L}_{ell} decomposes as a sum of expectations over individual data points thus stochastic optimization techniques can be used to evaluate this term making it independent of N . We provide an implementation of the algorithm that uses Tensorflow [1].

4 Related work

Our work is related to alternative multivariate formulations such as the linear coregionalization model (LCM) or the intrinsic coregionalization model (ICM) [3]. In the Bayesian treatment of LCM [22], the weight parameters are also stochastic and inference proceeds with MCMC. Another multivariate formulation is MLGCP [8, 24], which models the task-specific log-intensity as the sum of a shared GP and a task-specific GP while performing inference via the Metropolis-adjusted Langevin (MALA). These multivariate formulations of LGCP under MCMC and even INLA [21] approximations have been prohibitive due to computational cost [23], identifiability problems and slow convergence [8].

Modern advances in variational inference for models with GP priors and ‘black-box’ likelihoods have allowed the development of generic methods for inference in multivariate LGCPs [7, 18]. While these frameworks offer the opportunity to prototype new models quickly, they can only handle deterministic weights. In contrast, we exploit our model characteristics and derive closed-form expressions in the presence of stochastic weights that allow us to improve convergence and efficiency of the algorithm.

Finally, rather than using a GP prior over the log intensity, different transformations of the latent GPs have been considered as alternatives to model point data. For example, in the Permanental process, a GP prior is used over the squared root of the intensities [15–17, 27]. Similarly, a sigmoidal transformation of the latent GPs was studied by Adams et al. [2] and used in conjunction with convolution processes for modeling multi-output problems by Gunter et al. [11]).

Table 1: Results on the synthetic dataset when making predictions on the missing intervals. Our model is denoted by either LGCPN-N or LGCPN-GP according to whether the prior over the weights is uncorrelated or correlated, respectively. CPU time is given in seconds per epoch.

	RMSE				NLPL				CPU time
	1	2	3	4	1	2	3	4	
LGCPN-N	4.46	13.35	4.58	5.01	3.13	7.73	3.03	3.18	0.18
LGCPN-GP	4.34	14.82	4.46	4.58	3.81	7.68	3.14	2.96	0.25
LGCP [20]	11.06	17.63	7.80	14.06	26.44	30.92	20.88	32.37	0.32
ICM [12]	5.07	8.58	4.62	7.01	4.72	10.66	3.47	5.36	0.52

Table 2: RMSE and NLPL on BTB with missing data. Time in seconds per epoch.

	RMSE				NLPL (per cell)				CPU time
	GT 9	GT 12	GT 15	GT 20	GT 9	GT 12	GT 15	GT 20	
LGCPN-N	0.83 (0.15)	0.24 (0.07)	0.28 (0.07)	0.29 (0.10)	1.23 (0.40)	0.20 (0.07)	0.33 (0.11)	0.35 (0.16)	7.73
LGCPN-GP	0.81 (0.14)	0.22 (0.08)	0.27 (0.07)	0.27 (0.09)	1.42 (0.42)	0.27 (0.09)	0.41 (0.14)	0.58 (0.24)	7.63
LGCP [20]	1.37 (0.33)	0.61 (0.13)	0.63 (0.12)	1.24 (0.56)	1.70 (0.39)	0.48 (0.11)	0.72 (0.17)	0.86 (0.36)	8.76
ICM [12]	0.91 (0.15)	0.21 (0.07)	0.32 (0.08)	7.24 (5.48)	1.44 (0.40)	0.18 (0.06)	0.34 (0.10)	0.37 (0.14)	67.06

5 Experiments

We first conduct a preliminary analysis of LGCPN on a synthetic dataset. We then proceed to model two real world datasets that exhibit very different correlation structures. The first one includes tasks that are spatially segregated while the second one is characterized by strong positive correlation between tasks. We offer results on both complete and incomplete data settings while comparing against MLGCP [24], a variational LGCP model [20] and a variational formulation of ICM with Poisson likelihood implemented in GPflow [12, 18].¹

Synthetic data To illustrate the *transfer* capabilities of LGCPN we construct four correlated tasks by sampling from a multivariate point process with final intensities obtained as the linear combination of two latent functions via task-specific mixing weights (Fig. 2). When using a coupled prior over the weights, we consider covariates describing tasks (e.g. minimum and maximum values) as inputs. LGCPN is able to reconstruct the task intensities in the missing data regions by learning the inter-task correlation and transferring information across tasks. Importantly, it significantly outperforms competing approaches in terms of negative log predictive likelihood (NLPL) and has a lower root mean square error (RMSE) for $3/4$ of the tasks (Tab. 1) while being ≈ 3 times faster than ICM.

5.1 Bovine Tuberculosis (BTB) in Cornwall

In this section we demonstrate the performance, transfer capabilities and scalability of LGCPN on the bovine tuberculosis (BTB) dataset [8, 24]. The BTB dataset (Fig. 3, first row), consists of locations of BTB incidents in Cornwall, UK (period 1989–2002) and covariates measuring cattle density. We follow Diggle et al. [8] and only consider the four most common BTB genotypes (GT: 9, 12, 15 and 20). Lack of ground truth intensities typically restricts quantitative measures of generalization and hence we focus on validating and comparing LGCPN from two different perspectives: i) using complete data so as to assess the quality of the recovered intensities as well as the *computational complexity* and scalability gains over MLGCP; and ii) using missing data so as to validate the *transfer* capabilities of LGCPN when compared with LGCP and ICM.

¹Code for all the experiments is provided at XXXXXXXX

Complete Data Experiments: We estimate the four BTB intensities by fitting an LGCPN with four latent functions and Matérn 3/2 kernels. We initialise the kernel lengthscales and variances to 1. For direct comparison, we train the MLGCP model following the grid size, prior, covariance and MCMC settings by Taylor et al. [24]. We run the MCMC chain for 1M iterations with a burn in of 100K and keep 1K thinned steps. The resulting BTB intensities from LGCPN and MLGCP are presented in Fig. 3. Following Diggle et al. [8], we report the probability surfaces computed as $\pi_p(x) = \lambda_p(x) / \sum_{p=1}^P \lambda_p(x)$ where $\lambda_p(x)$ is the posterior mean of the intensity for task p at location x . Estimated intensities surfaces can be found in the supplementary material.

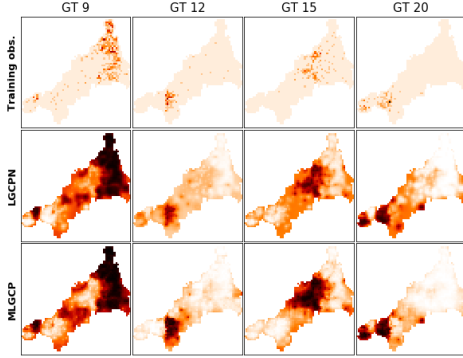


Figure 3: Estimated conditional probabilities on BTB (Second row: LGCPN, Third row:MLGCP) in the complete data setting. Estimated intensity surfaces are available in the supplementary material.

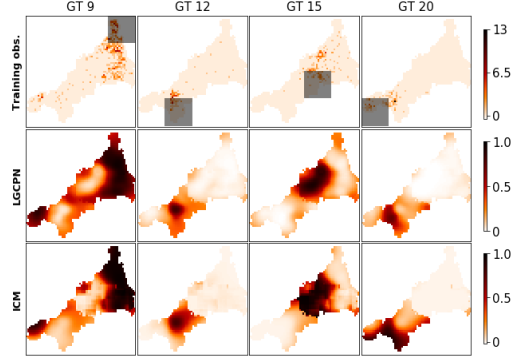


Figure 4: *First row:* Counts of the BTB incidents on a 64×64 grid. Shaded areas represent missing data regions. Estimated conditional probabilities by LGCPN (*second row*) and by ICM (*third row*).

The probability surfaces are comparable with both approaches characterizing well the high and low intensities albeit varying at the level of smoothness. We reproduce the MLGCP results by Taylor et al. [24] that we also report in the supplement using the same color spectrum as in the original paper. In terms of *computational gains* we note that MLGCP takes ≈ 30 hrs on a Intel Core i7-6t00U CPU (3.40GHz, 8GB of RAM) for an interpolation run on the four BTB tasks while LGCPN only requires ≈ 8 hrs. The previously reported [8] slow mixing and convergence problems of the chain, even after millions of MCMC iterations, renders MLGCP problematic for application to large-scale multivariate point processes. Finally, the built-in assumption of a single common GP latent process across tasks limits the number and the type of inter-task correlations that we can identify and model efficiently.

Missing Data Experiments: *Transfer* is evaluated by constructing missing data regions, see Fig. 4, and computing RMSE and NLPL performance metrics between the estimated intensity and the counts in these regions. We partition the spatial extend to 16 regions and create a missing data “fold” by combining 4 non-overlapping regions, one for each task. The shaded regions in Fig. 4 represent one such fold of the missing areas across tasks. We repeat the experiment 16 times until each task’s overall spatial extend is covered. We provide average quantitative metrics across folds for an LGCPN with four latent functions, Matérn 3/2 kernels and 30% of the training inputs as inducing inputs. As in the complete data setting, we report estimated conditional probabilities in Fig. 4. LGCPN manages to recover the overall behavior of the process in the missing regions showing significant transfer of information across spatially segregated tasks. LGCPN outperforms LGCP across all tasks and ICM on $3/4$ of the tasks (Tab. 2). In addition, LGCPN has a significant computational advance: it converges in 3.18 hrs (1500 epochs) while ICM converges in 18.63 hrs (1000 epochs).

5.2 Crime events in NYC

We showcase the performance of LGCPN on a second real-world dataset recording different crimes in New York City (CRIME). The dataset includes latitude and longitude locations of burglaries (1), felony assaults (2), grand larcenies (3), grand larcenies of motor vehicle (MV, 4), petit larcenies (5), petit larcenies of motor vehicle (MV, 6) and robberies (7) reported to the New York City Police Department (NYPD) in 2016. The data are discretized into a 32×32 regular grid (Fig. 5).

Complete/Missing Data Experiments We first consider full-data experiments and we spatially interpolate the crime surfaces running LGCPN with four latent functions characterized by Matérn 3/2

kernels. We repeat the experiment with MLGCP setting the parameters of the algorithm as suggested by Taylor et al. [24]. Similar results are obtained with the two methods (see Fig. (8) in the supplement for a visualisation of the estimated intensity surfaces). However, in terms of *computational gains*, an MLGCP run takes ≈ 14 hrs while LGCPN requires ≈ 2 hrs. In order to assess *transfer*, we keep

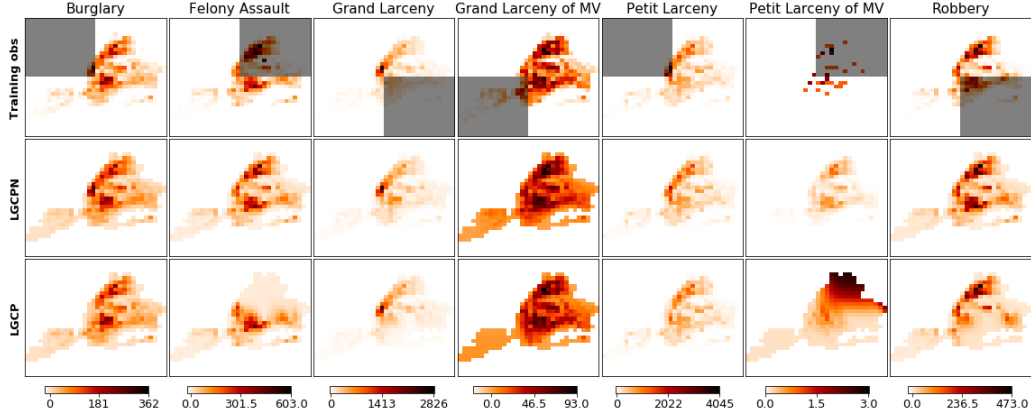


Figure 5: CRIME dataset. Estimated surface when introducing missing data in the shaded regions. Row 1: Counts of crime events on a regular grid. Row 2: LGCPN Row 3: LGCP.

the same experimental settings as above and we partition the spatial extent to 4 regions. We create missing data “folds” by combining 7 non-overlapping regions, one for each task. We first place the missing region for “Burglary” in the upper left corner of the grid and we move forward this missing region 4 times until the overall area is covered. The shaded regions in Fig. 5 represent one possible configuration of the missing data across tasks. Overall, we cover the complete spatial extent of each task thus accounting for areas of both high and low intensity. LGCPN successfully transfers information across tasks (Fig. 5) thereby recovering, for all crime types, the signal in the missing data regions. The algorithm captures the high and low intensity areas by exploiting task similarities. LGCPN outperforms competing approaches in all of the tasks, both in terms of NLPL (Tab. 3) and in terms of RMSE (see the supplementary material.) Finally, LGCPN significantly outruns ICM in terms of algorithm efficiency. LGCPN-N converges in 1.19 hrs (1500 epochs) while ICM needs 12.26 hrs (1000 epochs).

Table 3: CRIME dataset. Performance on the missing regions. Time in seconds per epoch.

	Standardized NLPL (per cell)							CPU time
	1	2	3	4	5	6	7	
LGCPN	0.56 (0.10)	0.91 (0.27)	0.66 (0.30)	1.09 (0.27)	0.85 (0.52)	10.29 (2.51)	0.42 (0.05)	2.85
LGCPN-GP	0.72 (0.18)	0.75 (0.18)	0.94 (0.55)	1.53 (0.52)	0.57 (0.19)	18.76 (8.25)	0.58 (0.12)	3.11
LGCP [20]	9.90 (3.66)	9.32 (2.41)	19.34 (11.45)	5.30 (1.02)	18.18 (8.65)	36.73 (4.02)	9.68 (2.67)	2.87
ICM [12]	0.87 (0.27)	1.36 (0.35)	0.91 (0.45)	1.19 (0.40)	0.69 (0.11)	12.30 (3.02)	0.93 (0.17)	44.13

6 Conclusions and Discussion

We propose a new multi-task learning framework for modeling correlated count data based on LGCP models. We consider observations on different tasks as being drawn from distinct LGCPs with correlated intensities determined by linearly combined GPs through task-specific random weights. By considering stochastic weights, we allow for the incorporation of additional dependencies across

tasks while providing a better uncertainty quantification. We derive closed-form expressions for the moments of the intensity functions and use them to develop an efficient variational algorithm that is order of magnitude faster than the current state of the art. We show how LGCPN achieves the state of the art performance on both synthetic and real datasets providing a more flexible and on average 9 times faster methodology compared to the available LGCPN multivariate methods. Future work will focus on increasing the interpretability of the mixing weights by using sparse priors such as those considered in [26].

Acknowledgments This work was supported by the EPSRC grant EP/L016710/1 and The Alan Turing Institute under EPSRC grant EP/N510129/1 as well as the Lloyds Register Foundation programme on Data Centric Engineering.

References

- [1] Abadi, M., Agarwal, A., Barham, P., Brevdo, E., Chen, Z., Citro, C., Corrado, G. S., Davis, A., Dean, J., Devin, M., et al. (2016). Tensorflow: Large-scale machine learning on heterogeneous distributed systems. *arXiv preprint arXiv:1603.04467*.
- [2] Adams, R. P., Murray, I., and MacKay, D. J. (2009). Tractable nonparametric bayesian inference in poisson processes with gaussian process intensities. In *Proceedings of the 26th Annual International Conference on Machine Learning*, pages 9–16. ACM.
- [3] Alvarez, M. A., Rosasco, L., and Lawrence, N. D. (2011). Kernels for vector-valued functions: a review. URL <http://arxiv.org/abs/1106.6251>.
- [4] Bonilla, E. V., Krauth, K., and Dezfouli, A. (2016). Generic inference in latent Gaussian process models. *arXiv preprint arXiv:1609.00577*.
- [5] Cox, D. R. (1955). Some statistical methods connected with series of events. *Journal of the Royal Statistical Society. Series B (Methodological)*, pages 129–164.
- [6] Craig, C. C. (1936). On the frequency function of xy . *The Annals of Mathematical Statistics*, 7(1):1–15.
- [7] Dezfouli, A. and Bonilla, E. V. (2015). Scalable inference for Gaussian process models with black-box likelihoods. pages 1414–1422.
- [8] Diggle, P. J., Moraga, P., Rowlingson, B., and Taylor, B. M. (2013). Spatial and spatio-temporal log-gaussian cox processes: Extending the geostatistical paradigm. *Statistical Science*, pages 542–563.
- [9] Flaxman, S., Wilson, A., Neill, D., Nickisch, H., and Smola, A. (2015). Fast kronecker inference in gaussian processes with non-gaussian likelihoods. In *International Conference on Machine Learning*, pages 607–616.
- [10] Gomes, C. P. (2009). Computational sustainability: Computational methods for a sustainable environment, economy, and society. *The Bridge*, 39(4):5–13.
- [11] Gunter, T., Lloyd, C., Osborne, M. A., and Roberts, S. J. (2014). Efficient bayesian nonparametric modelling of structured point processes. *arXiv preprint arXiv:1407.6949*.
- [12] Hensman, J., Matthews, A., and Ghahramani, Z. (2015). Scalable variational Gaussian process classification. In *Artificial Intelligence and Statistics*.
- [13] Jordan, M. I., Ghahramani, Z., Jaakkola, T. S., and Saul, L. K. (1999). An introduction to variational methods for graphical models. *Machine learning*, 37(2):183–233.
- [14] Leininger, T. J., Gelfand, A. E., et al. (2017). Bayesian inference and model assessment for spatial point patterns using posterior predictive samples. *Bayesian Analysis*, 12(1):1–30.
- [15] Lian, W., Henao, R., Rao, V., Lucas, J., and Carin, L. (2015). A multitask point process predictive model. In *International Conference on Machine Learning*, pages 2030–2038.

- [16] Lloyd, C., Gunter, T., Nickson, T., Osborne, M., and Roberts, S. J. (2016). Latent point process allocation.
- [17] Lloyd, C., Gunter, T., Osborne, M. A., and Roberts, S. J. (2015). Variational Inference for Gaussian Process Modulated Poisson Processes. In *International Conference on Machine Learning*.
- [18] Matthews, A. G. d. G., van der Wilk, M., Nickson, T., Fujii, K., Boukouvalas, A., León-Villagrà, P., Ghahramani, Z., and Hensman, J. (2017). GPflow: A Gaussian process library using TensorFlow. *Journal of Machine Learning Research*, 18(40):1–6.
- [19] Møller, J., Syversveen, A. R., and Waagepetersen, R. P. (1998). Log gaussian cox processes. *Scandinavian journal of statistics*, 25(3):451–482.
- [20] Nguyen, T. V. and Bonilla, E. V. (2014). Automated variational inference for Gaussian process models. pages 1404–1412.
- [21] Rue, H., Martino, S., and Chopin, N. (2009). Approximate bayesian inference for latent gaussian models by using integrated nested laplace approximations. *Journal of the royal statistical society: Series b (statistical methodology)*, 71(2):319–392.
- [22] Schmidt, A. M. and Gelfand, A. E. (2003). A bayesian coregionalization approach for multivariate pollutant data. *Journal of Geophysical Research: Atmospheres*, 108(D24).
- [23] Shirota, S. and Gelfand, A. E. (2016). Inference for log Gaussian Cox processes using an approximate marginal posterior. *arXiv preprint arXiv:1611.10359*.
- [24] Taylor, B., Davies, T., Rowlingson, B., and Diggle, P. (2015). Bayesian inference and data augmentation schemes for spatial, spatiotemporal and multivariate log-Gaussian Cox processes in r. *Journal of Statistical Software*, 63:1–48.
- [25] Titsias, M. K. (2009). Variational learning of inducing variables in sparse gaussian processes. 5:567–574.
- [26] Titsias, M. K. and Lázaro-Gredilla, M. (2011). Spike and slab variational inference for multi-task and multiple kernel learning. pages 2339–2347.
- [27] Walder, C. J. and Bishop, A. N. (2017). Fast Bayesian intensity estimation for the permanental process. In *International Conference on Machine Learning*.
- [28] Williams, C. K. and Rasmussen, C. E. (2006). Gaussian processes for machine learning. *the MIT Press*, 2(3):4.

Supplementary Material

1 Plate diagrams

Here we provide the plate diagrams for LGCPN:

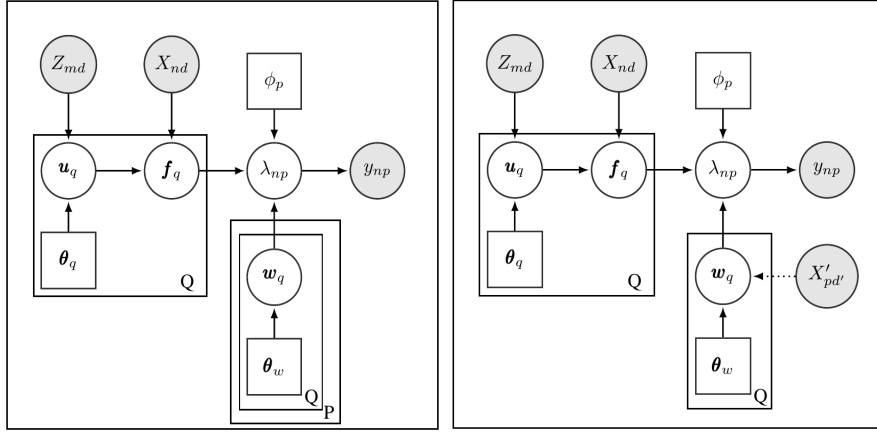


Figure 1: *Left plot:* LGCPN-N. When placing a Normal prior on each w_{pq} , we introduce the additional factorization across P . *Right plot:* LGCPN-GP $X'_{pd'}$ represents the inputs for the GP prior on \mathbf{W} .

2 Derivation of the KL-divergence Term

The KL-divergence terms composing the ELBO can be written as:

$$\mathcal{L}_{\text{ent}}^u(\boldsymbol{\nu}_u) = \frac{1}{2} \sum_{q=1}^Q [M \log 2\pi + \log |\mathbf{S}_q| + M] \quad (1)$$

$$\mathcal{L}_{\text{cross}}^u(\boldsymbol{\nu}_u) = \sum_{q=1}^Q \left[\log \mathcal{N}(\mathbf{m}_q; \mathbf{0}, \mathbf{K}_{zz}^q) - \frac{1}{2} \text{tr}(\mathbf{K}_{zz}^q)^{-1} \mathbf{S}_q \right] \quad (2)$$

$$\mathcal{L}_{\text{cross}}^w(\boldsymbol{\nu}_w) = \sum_{q=1}^Q \left[\log \mathcal{N}(\boldsymbol{\omega}_q; \mathbf{0}, \mathbf{K}_w^q) - \frac{1}{2} \text{tr}(\mathbf{K}_w^q)^{-1} \boldsymbol{\Omega}_q \right] \quad (3)$$

$$\mathcal{L}_{\text{ent}}^w(\boldsymbol{\nu}_w) = \frac{1}{2} \sum_{q=1}^Q [P \log 2\pi + \log |\boldsymbol{\Omega}_q| + P], \quad (4)$$

When placing an independent prior and approximate posterior over \mathbf{W} , the terms $\mathcal{L}_{\text{ent}}^w$ and $\mathcal{L}_{\text{cross}}^w$ get simplified further, reducing the computational cost significantly when a large number of tasks is considered. Here we derive the expressions for Eqs. (1)–(4).

The entropy term for \mathbf{U} (Eq. (1)) is given by:

$$\begin{aligned}
\mathcal{L}_{\text{ent}}^u(\boldsymbol{\nu}_u) &= -\mathbb{E}_{q(\mathbf{U}|\boldsymbol{\nu}_u)}[\log q(\mathbf{U}|\boldsymbol{\nu}_u)] \\
&= -\int q(\mathbf{U}|\boldsymbol{\nu}_u) \log q(\mathbf{U}|\boldsymbol{\nu}_u) d\mathbf{U} \\
&= -\sum_{q=1}^Q \int q(\mathbf{U}_{\bullet q}|\boldsymbol{\nu}_u) \log q(\mathbf{U}_{\bullet q}|\boldsymbol{\nu}_u) d\mathbf{U}_{\bullet q} \\
&= -\sum_{q=1}^Q \int \mathcal{N}(\mathbf{U}_{\bullet q}; \mathbf{m}_q, \mathbf{S}_q) \log \mathcal{N}(\mathbf{U}_{\bullet q}; \mathbf{m}_q, \mathbf{S}_q) d\mathbf{U}_{\bullet q} \\
&= -\sum_{q=1}^Q \left[\mathcal{N}(\mathbf{m}_q; \mathbf{m}_q, \mathbf{S}_q) - \frac{1}{2} \text{tr}(\mathbf{S}_q)^{-1} \mathbf{S}_q \right] \\
&= \frac{1}{2} \sum_{q=1}^Q [M \log 2\pi + \log |\mathbf{S}_q| + M].
\end{aligned}$$

The cross-entropy term for \mathbf{U} (Eq. (2)) is given by:

$$\begin{aligned}
\mathcal{L}_{\text{cross}}^u(\boldsymbol{\nu}_u) &= \mathbb{E}_{q(\mathbf{U}|\boldsymbol{\nu}_u)}[\log p(\mathbf{U})] \\
&= \int q(\mathbf{U}|\boldsymbol{\nu}_u) \log p(\mathbf{U}) d\mathbf{U} \\
&= \sum_{q=1}^Q \int q(\mathbf{U}_{\bullet q}|\boldsymbol{\nu}_u) \log p(\mathbf{U}_{\bullet q}) d\mathbf{U}_{\bullet q} \\
&= \sum_{q=1}^Q [\mathcal{N}(\mathbf{U}_{\bullet q}; \mathbf{m}_q, \mathbf{S}_q) \log \mathcal{N}(\mathbf{U}_{\bullet q}; \mathbf{0}, \mathbf{K}_{zz}^q)] \\
&= \sum_{q=1}^Q \left[\log \mathcal{N}(\mathbf{m}_q; \mathbf{0}, \mathbf{K}_{zz}^q) - \frac{1}{2} \text{tr}(\mathbf{K}_{zz}^q)^{-1} \mathbf{S}_q \right].
\end{aligned}$$

When placing a coupled prior on the mixing weights, the entropy term for \mathbf{W} (Eq. (3)) is given by:

$$\begin{aligned}
\mathcal{L}_{\text{ent}}^w(\boldsymbol{\nu}_w) &= -\int q(\mathbf{W}|\boldsymbol{\nu}_w) \log q(\mathbf{W}|\boldsymbol{\nu}_w) d\mathbf{W} \\
&= -\sum_{q=1}^Q \int \mathcal{N}(\mathbf{W}_{\bullet q}; \boldsymbol{\omega}_q, \boldsymbol{\Omega}_q) \log \mathcal{N}(\mathbf{W}_{\bullet q}; \boldsymbol{\omega}_q, \boldsymbol{\Omega}_q) d\mathbf{W}_{\bullet q} \\
&= -\sum_{q=1}^Q \left[\mathcal{N}(\boldsymbol{\omega}_q; \boldsymbol{\omega}_q, \boldsymbol{\Omega}_q) - \frac{1}{2} \text{tr}(\boldsymbol{\Omega}_q)^{-1} \boldsymbol{\Omega}_q \right] \\
&= \frac{1}{2} \sum_{q=1}^Q [P \log 2\pi + \log |\boldsymbol{\Omega}_q| + P].
\end{aligned}$$

The cross-entropy term for \mathbf{W} (Eq. (4)) is given by:

$$\begin{aligned}
\mathcal{L}_{\text{cross}}^w(\boldsymbol{\nu}_w) &= \mathbb{E}_{q(\mathbf{W}|\boldsymbol{\nu}_w)}[\log p(\mathbf{W})] \\
&= \int q(\mathbf{W}|\boldsymbol{\nu}_w) \log p(\mathbf{W}) d\mathbf{W} \\
&= \sum_{q=1}^Q \int q(\mathbf{W}_{\bullet q}|\boldsymbol{\nu}_w) \log p(\mathbf{W}_{\bullet q}) d\mathbf{W}_{\bullet q} \\
&= \sum_{q=1}^Q \int \mathcal{N}(\mathbf{W}_{\bullet q}; \boldsymbol{\omega}_q, \boldsymbol{\Omega}_q) \log \mathcal{N}(\mathbf{W}_{\bullet q}; \mathbf{0}, \mathbf{K}_w^q) d\mathbf{W}_{\bullet q} \\
&= \sum_{q=1}^Q \left[\log \mathcal{N}(\boldsymbol{\omega}_q; \mathbf{0}, \mathbf{K}_w^q) - \frac{1}{2} \text{tr}(\mathbf{K}_w^q)^{-1} \boldsymbol{\Omega}_q \right].
\end{aligned}$$

When placing an independent prior and approximate posterior over \mathbf{W} , the terms $\mathcal{L}_{\text{ent}}^w$ and $\mathcal{L}_{\text{cross}}^w$ get further simplified in:

$$\begin{aligned}
\mathcal{L}_{\text{ent}}^w(\boldsymbol{\nu}_w) &= - \int q(\mathbf{W}|\boldsymbol{\nu}_w) \log q(\mathbf{W}|\boldsymbol{\nu}_w) d\mathbf{W} \\
&= - \sum_{q=1}^Q \sum_{p=1}^P \int \mathcal{N}(w_{pq}; \omega_{pq}, \Omega_{pq}) \log \mathcal{N}(w_{pq}; \omega_{pq}, \Omega_{pq}) dw_{pq} \\
&= \frac{1}{2} \sum_{q=1}^Q \sum_{p=1}^P [\log 2\pi + \log \Omega_{pq} + 1],
\end{aligned}$$

and in:

$$\begin{aligned}
\mathcal{L}_{\text{cross}}^w(\boldsymbol{\nu}_w) &= \int q(\mathbf{W}|\boldsymbol{\nu}_w) \log p(\mathbf{W}) d\mathbf{W} \\
&= \sum_{q=1}^Q \sum_{p=1}^P \int q(w_{pq}|\boldsymbol{\nu}_w) \log p(w_{pq}) dw_{pq} \\
&= \sum_{q=1}^Q \sum_{p=1}^P \int \mathcal{N}(w_{pq}; \omega_{pq}, \Omega_{pq}) \log \mathcal{N}(w_{pq}; \mathbf{0}, \sigma_{pq}^2) dw_{pq} \\
&= \sum_{q=1}^Q \sum_{p=1}^P \left[\log \mathcal{N}(\omega_{pq}; \mathbf{0}, \Omega_{pq}) - \frac{\Omega_{pq}}{2\sigma_{pq}^2} \right],
\end{aligned}$$

where Ω_{pq} represents the p -th diagonal term of $\boldsymbol{\Omega}_q$.

3 Closed form evaluation of the ELL term

The LGCPN model formulation allows to derive a closed form expression for the moments of the intensity function. Here we provide details about the derivation and obtain an expression for the first moment which has been used in the closed form evaluation of \mathcal{L}_{ell} .

In order to compute the moments of λ we can exploit the moment generating function (MGF) of the product of two normal random variables. Denote by X and Y two independent and normally distributed random variables. The variable $Z = XY$ has MGF $_Z(t)$ defined as:

$$\text{MGF}_Z(t) = \frac{\exp \left[\frac{t\mu_X\mu_Y + 1/2(\mu_Y^2\sigma_X^2 + \mu_X^2\sigma_Y^2)t^2}{1-t^2\sigma_X^2\sigma_Y^2} \right]}{\sqrt{1-t^2\sigma_X^2\sigma_Y^2}} \quad (5)$$

Now define $V = \sum_{q=1}^Q X_q Y_q$ where $X_q \perp\!\!\!\perp Y_q, \forall q$ and $X_q \perp\!\!\!\perp X_{q'}, \forall q, q'$ and $Y_q \perp\!\!\!\perp Y_{q'}, \forall q, q'$. Given the independent assumption, the MGF for V is defined as the product of Q MGF of the form given in Eq. (5). We have: that $\text{MGF}_V(t) = \prod_{q=1}^Q \text{MGF}_{Z_q}(t)$.

This implies that:

$$\mathbb{E}(\lambda_p) = \mathbb{E}[\exp(\mathbf{W}_{p\bullet} \mathbf{F}_{n\bullet})] = \text{MGF}_V(1) \quad (6)$$

where $X_q = \omega_{pq}$ and $Y_q = f_{nq}$.

Exploiting Eq. (6) we can derive a closed form expression for \mathcal{L}_{ell} :

$$\begin{aligned} \mathbb{E}_{q(\mathbf{F}), q(\mathbf{W})} [\log(p(\mathbf{Y}|\mathbf{F}, \mathbf{W}))] &= \sum_{n=1}^N \sum_{p=1}^P \mathbb{E}[-\exp(\mathbf{W}_{p\bullet} \mathbf{F}_{n\bullet} + \phi_p) + y_{np} \log(\exp(\mathbf{W}_{p\bullet} \mathbf{F}_{n\bullet} + \phi_p) + \log\Gamma(y_{np} + 1))] \\ &= \sum_{n=1}^N \sum_{p=1}^P \mathbb{E}[-\exp(\mathbf{W}_{p\bullet} \mathbf{F}_{n\bullet} + \phi_p) + y_{np} \mathbf{W}_{p\bullet} \mathbf{F}_{n\bullet} + y_{np} \phi_p + \log\Gamma(y_{np} + 1)] \\ &= - \sum_{n=1}^N \sum_{p=1}^P \mathbb{E}[\exp(\mathbf{W}_{p\bullet} \mathbf{F}_{n\bullet} + \phi_p)] + \sum_{n=1}^N \sum_{p=1}^P [y_{np} \mathbb{E}(\mathbf{W}_{p\bullet} \mathbf{F}_{n\bullet}) + y_{np} \phi_p + \log\Gamma(y_{np} + 1)] \\ &= - \sum_{n=1}^N \sum_{p=1}^P \exp(\phi_p) \text{MGF}_V(1) + \sum_{n=1}^N \sum_{p=1}^P \sum_{q=1}^Q (y_{np} \omega_{pq} \mu_q(\mathbf{x}_n) + y_{np} \phi_p + \log\Gamma(y_{np} + 1)) \quad (7) \end{aligned}$$

Given the moments of $q(\mathbf{W}_{p\bullet})$ and $q(\mathbf{F}_{n\bullet})$ we can write:

$$\mathbb{E}_{q(\mathbf{F}_{n\bullet}), q(\mathbf{W}_{p\bullet})} [\exp(\mathbf{W}_{p\bullet} \mathbf{F}_{n\bullet})] = \prod_{q=1}^Q \frac{\exp\left[\frac{\omega_{pq} \mu_{nq} + 1/2(\mu_{nq}^2 \Omega_{pq} + \omega_{pq}^2 \Sigma_{nn}^q)}{1 - \Omega_{pq} \Sigma_{nn}^q}\right]}{\sqrt{1 - \Omega_{pq} \Sigma_{nn}^q}} \quad (8)$$

Defining $\delta_X = \mu_X / \sigma_X$ in Eq. (5) we can rewrite $\text{MGF}_Z(t)$ as:

$$\text{MGF}_Z(t) = \frac{\exp\left[\frac{t\mu_X \mu_Y + 1/2(\mu_Y^2 \sigma_X^2 + \mu_X^2 \sigma_Y^2)t^2}{1 - t^2 \frac{\mu_X^2 \sigma_Y^2}{\delta_X^2}}\right]}{\sqrt{1 - t^2 \frac{\mu_X^2 \sigma_Y^2}{\delta_X^2}}} \quad (9)$$

As δ_X increases, $\text{MGF}_Z(t)$ converges to the form:

$$\text{MGF}_Z(t) = \exp[t\mu_X \mu_Y + 1/2(\mu_Y^2 \sigma_X^2 + \mu_X^2 \sigma_Y^2)t^2] \quad (10)$$

which is the MGF of a Gaussian distribution with mean and variance given by $\mu_X \mu_Y$ and $\mu_Y^2 \sigma_X^2 + \mu_X^2 \sigma_Y^2$ respectively [2]. This implies that, for increasing values of δ_{X_q} the sum of the products of Gaussians tends to a Gaussian distribution.

In turns this means that, as $\Omega_q \rightarrow 0$, $\mathbf{W}_{p\bullet} \mathbf{F}_{n\bullet}$ converges to a Gaussian distribution. Depending on the number of latent GPs included in the model (Q) and the moments of $q(\mathbf{W}_{p\bullet})$, LGCPN will thus converge either to an ICM (or LCM) or to a MLGCP or to an LGCP. When $Q \neq P$, we have $\log \lambda_p(\mathbf{x}_n) = \sum_{q=1}^Q \omega_{pq} \mathbf{F}_{n\bullet}$ for each n and p . We can thus write:

$$\begin{aligned} \lim_{\mathbf{K}_w \rightarrow 0} \text{Cov}(\log \lambda_p(\mathbf{x}), \log \lambda_{p'}(\mathbf{x}')) &= \sum_{q=1}^Q \sum_{q'=1}^Q \omega_{pq} \omega_{p'q'} \text{Cov}(\mathbf{F}_{\bullet q}, \mathbf{F}_{\bullet q'}) \\ &= \sum_{q=1}^Q \underbrace{\omega_{pq} \omega_{p'q'}}_{\mathbf{B}_q} \tilde{\mathbf{K}}_{\mathbf{x}\mathbf{x}'}^q \end{aligned}$$

where we have exploited the independence assumption between $\mathbf{F}_{\bullet q}$ and $\mathbf{F}_{\bullet q'}$ for $q \neq q'$ [?].

When $Q = P + 1$ and $\mathbf{W}_{P \times (P+1)} = [\mathbf{I}_P \ \mathbb{1}_P]$, the intensity for each task will be determined by the $(P + 1)$ -th common GP and by the p -th task specific GP. We thus recover the MLGCP formulation.

Finally, when $Q = P$ and $\mathbf{W}_{P \times P} = \mathbf{I}_P$, the intensity for each task will be determined only by the p -th task specific GP. We thus recover the LGCP formulation.

4 Continuous LGCPN formulation

Following a common approach, in our work we introduce a computational grid on the spatial extend and consider the cells' centroids as inputs of LGCPN. Here we discuss an alternative continuous formulation of our model. The likelihood function for the continuous LGCPN model can be written as:

$$p(Y|\lambda) = \exp \left[- \sum_{p=1}^P \int_{\tau} \lambda_p(\mathbf{x}) d\mathbf{x} \right] \prod_{p=1}^P \prod_{n_p} \lambda_p(\mathbf{x}_{n_p})$$

where n_p indicates the location of the n -th event for the p -th task. This implies an expected log likelihood term defined as:

$$\mathbb{E}_{q(\mathbf{F})q(\mathbf{W})} \left[- \sum_p \int_{\tau} \lambda_p(\mathbf{x}) d\mathbf{x} + \sum_{p=1}^P \sum_{n_p} \log \lambda_p(\mathbf{x}_{n_p}) \right]$$

Replacing the expression for LGCPN intensity in the previous equation we get:

$$\begin{aligned} \mathbb{E}_{q(\mathbf{F})q(\mathbf{W})} \log(p(Y|\lambda)) &= - \sum_{p=1}^P \int_{\tau} \int_{\mathbf{F}} \int_{\mathbf{W}} \exp \left(\sum_{q=1}^Q w_p f(\mathbf{x}) \right) q(\mathbf{W}) q(\mathbf{F}) d\mathbf{W} d\mathbf{F} d\mathbf{x} + \\ &+ \sum_{p=1}^P \sum_{n_p} \int_{\tau} \int_{\mathbf{F}} \int_{\mathbf{W}} \log \left[\exp \left(\sum_{q=1}^Q w_p f(\mathbf{x}_{n_p}) \right) \right] q(\mathbf{W}) q(\mathbf{F}) d\mathbf{W} d\mathbf{F} \\ &= - \sum_{p=1}^P \int_{\tau} \mathbb{E} \left[\exp \left(\sum_{q=1}^Q w_p f(\mathbf{x}) \right) \right] d\mathbf{x} \\ &+ \sum_{p=1}^P \sum_{n_p} \int_{\tau} \int_{\mathbf{F}} \int_{\mathbf{W}} \sum_{q=1}^Q w_p f(\mathbf{x}_{n_p}) q(\mathbf{W}) q(\mathbf{F}) d\mathbf{W} d\mathbf{F} d\mathbf{x} \\ &= - \sum_{p=1}^P \int_{\tau} \mathbb{E} \left[\exp \left(\sum_{q=1}^Q w f(\mathbf{x}) \right) \right] d\mathbf{x} + \sum_{p=1}^P \sum_{n_p} \mathbb{E} \left(\sum_{q=1}^Q w_p f(\mathbf{x}_{n_p}) \right) \end{aligned}$$

for a bounded region τ . The expected value of $\exp(\mathbf{W}_{p\bullet} \mathbf{F}_{n\bullet})$ can be computed as in Eq. 8 while $\mathbb{E}_{q(\mathbf{F})q(\mathbf{W})} (\sum_{q=1}^Q w_p f(\mathbf{x}_{n_p}))$ is equal to:

$$\mathbb{E}_{q(\mathbf{F})q(\mathbf{W})} \left(\sum_{q=1}^Q w_p f(\mathbf{x}_{n_p}) \right) = \sum_{q=1}^Q \omega_p \mu_q(\mathbf{x}_{n_p}) \quad (11)$$

We are thus left with an intractable integral of the form:

$$- \sum_{p=1}^P \left[\prod_{q=1}^Q \frac{1}{\sqrt{1 - \Omega_{pq}^2 \Sigma_{nn}^q}} \exp \left(- \frac{\omega_{pq}^2}{2\Omega_{pq}^2} \right) \int_{\tau} \exp \left(\frac{(\Omega_{pq}^2 \mu_q(\mathbf{x}) + \omega_{pq})^2}{\Omega_{pq}^2 \Sigma_{nn}^q - 1} \right) d\mathbf{x} \right]$$

where the posterior mean for $q(\mathbf{F})$ computed in \mathbf{x} is defined as $\mu_q(\mathbf{x}) = k_{xz}^q (K_{zz})^{-1} m_q$.

This integral could be approximated using a series expansion but this would result in a computationally difficult problem.

5 Pseudo-algorithm

Algorithm 1 illustrates the LGCPN algorithm:

Algorithm 1 LGCPN

- 1: **Inputs:** Observational dataset $\mathcal{D} = \{\mathbf{x}_p^{(i)} \in \tau, \forall p = 1, \dots, P\}_{i=1}^I$ for bounded region τ where I denotes the number of events. Number of latent GPS Q . Number of mini-batches b of size B .
 - 2: **Output:** Optimized hyper-parameters, posterior moments of λ
 - 3:
 - 4: Discretize event locations \mathcal{D} in $Y \in \mathbb{R}^{N \times P}$ given the grid size.
 - 5: **Initialize:** $i \leftarrow 0, \eta^{(0)} = (\theta, \theta_w, \phi, \nu_u, \nu_w)$
 - 6: **repeat**
 - 7: $\{X_{train} \in \mathbb{R}^{B \times D}, Y_{train} \in \mathbb{R}^{B \times P}\} \rightarrow \text{get-next-MiniBatch}(\mathcal{D})$
 - 8: **for** $j=0$ to b **do**
 - 9: $\max_{\mu} \mathcal{L}_{\text{elbo}}(\eta^{(i)})$ (Eqs. (1)–(4) and (7))
 - 10: $\eta^{(i)} \leftarrow \eta^{(i-1)} - \rho \nabla_{\eta} \mathcal{L}_{\text{elbo}}(\eta^{(i-1)})$
 - 11: $i = i + 1$
 - 12: **end for**
 - 13: **until** convergence criterion is met.
 - 14: $\eta^* \leftarrow \eta^{(i-1)}$
 - 15: $\mathbb{E}[\lambda(\mathbf{x})^t] = \exp(t\phi^*) \text{MGF}_{\mathbf{WF}}|_{\eta^*}(t)$
-

6 Algorithmic efficiency

Evaluating \mathcal{L}_{ell} in closed form, we are able to significantly speed up the algorithm by getting rid of the Monte Carlo evaluations, see Fig. 2 and Fig. 3.

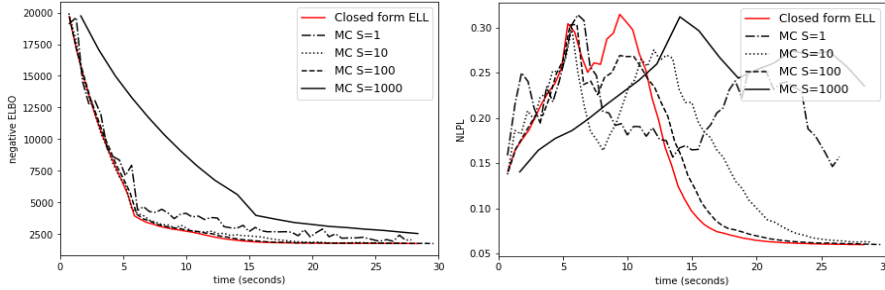


Figure 2: Synthetic data. MC estimate of ELL vs. Closed form evaluation of ELL. *Left:* Negative ELBO values over time. *Right:* NLPL values for one task over time. S denotes the number of samples used in the MC evaluation.

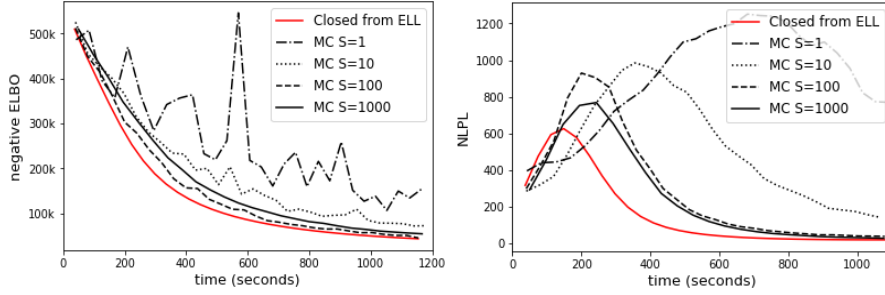


Figure 3: CRIME data. MC estimate of ELL vs. Closed form evaluation of ELL. *Left*: Negative ELBO values over time. *Right*: NLPL values for one task over time. S denotes the number of samples used in the MC evaluation.

7 Additional Details of Experiments

Performance comparisons are based on RMSE and NLPL values. RMSE values for the p -th task are computed as $\text{RMSE}_p = \sqrt{\frac{1}{N} \sum_{n=1}^N (y_{np} - \mathbb{E}(\lambda_{np}))^2}$ where $\mathbb{E}(\lambda_{np})$ represents the posterior mean estimate for the p -th intensity at \mathbf{x}_n . In order to account for both posterior mean and posterior variance of λ , we compute NLPL by sampling S values from the variational distributions $q(\mathbf{F})$ and $q(\mathbf{W})$ and averaging the predictive likelihood for each sample:

$$\text{NLPL}_p = -\frac{1}{S} \sum_{s=1}^S \frac{\sum_{n=1}^N \log p(y_{np} | \lambda_{np}^s)}{n}$$

7.1 Synthetic data experiments

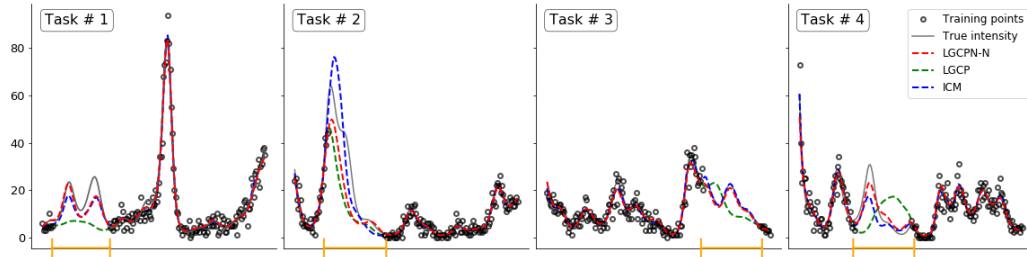


Figure 4: Four related tasks evaluated at 200 evenly spaced points in $[-1.5, 1.5]$. $| \cdot |$ denote the 50 contiguous observations removed from the training set of each task.

7.2 BTB data experiments

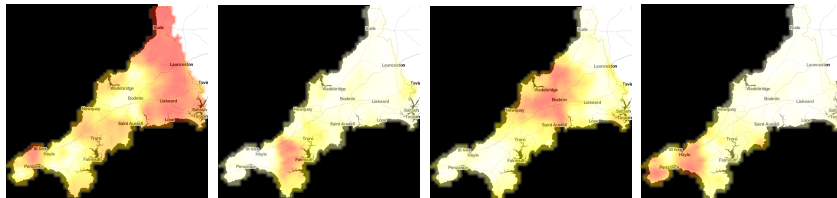


Figure 5: MLGCP- BTB dataset. Estimated conditional probabilities plotted on the color scale used by Diggle et al. [1] and Taylor et al. [3]. The first plots corresponds to GT 9, the second to GT 12, the third to GT 15 and the fourth to GT 20.

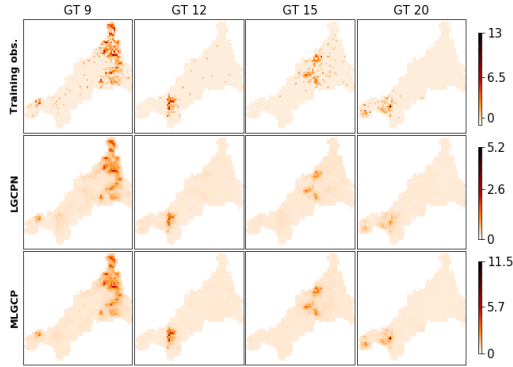


Figure 6: Estimated intensity surfaces in the complete data setting. *First row: Training data. Second row: LGCPN Third row: MLGCP*

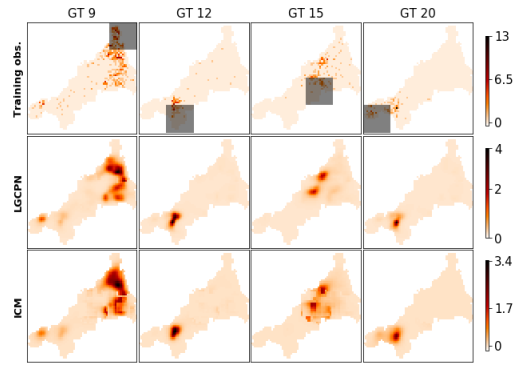


Figure 7: Estimated intensity surfaces in the missing data (shaded regions) setting. *First row: Training data. Second row: LGCPN Third row: ICM*

7.3 Crime data experiments

Table 1: CRIME dataset. Performance on the missing regions. Standard errors in parentheses.

Method \ Crime type #	Standardized RMSE						
	1	2	3	4	5	6	7
LGCPN	1.74 (0.42)	2.91 (1.06)	3.00 (1.22)	2.75 (0.82)	3.57 (1.99)	11.70 (2.32)	1.54 (0.29)
LGCPN-GP	1.71 (0.39)	1.91 (0.33)	3.40 (1.80)	2.96 (1.03)	2.00 (0.47)	12.18 (2.76)	1.62 (0.33)
LGCP	5.16 (1.81)	4.68 (0.99)	8.93 (5.22)	3.09 (0.50)	7.69 (3.68)	36.96 (5.43)	5.19 (1.21)
ICM	3.36 (1.04)	3.64 (0.83)	3.70 (1.89)	2.97 (1.22)	3.05 (0.97)	12.36 (1.99)	2.82 (0.62)

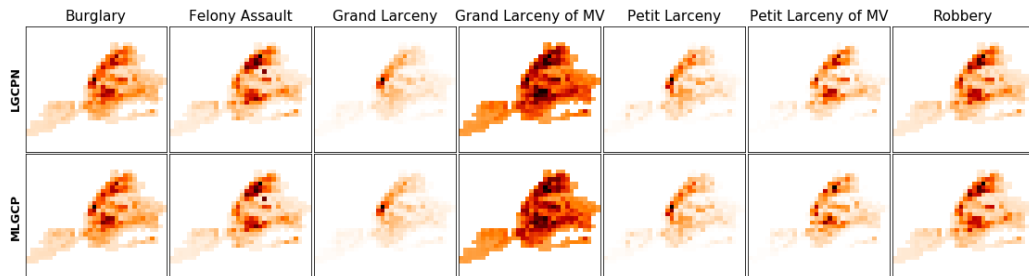


Figure 8: CRIME dataset. Estimated intensity surface with LGCPN (*first row*) and MLGCP (*second row*). The color scale used for each crime is given in Fig. (5).

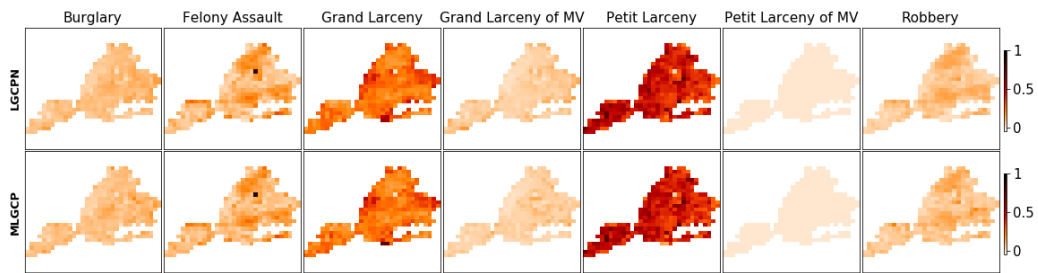


Figure 9: CRIME dataset. Estimated conditional probabilities in the complete data setting. *Row 1:* LGCPN *Row 2:* MLGCP.

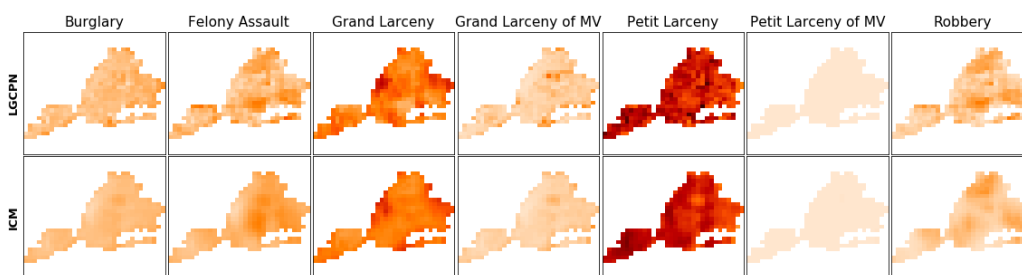


Figure 10: CRIME dataset. Estimated conditional probabilities when introducing missing data regions. *Row 1:* LGCPN *Row 2:* LGCP.

References

- [1] Diggle, Peter J, Moraga, Paula, Rowlingson, Barry, and Taylor, Benjamin M. Spatial and spatio-temporal log-gaussian cox processes: Extending the geostatistical paradigm. *Statistical Science*, pp. 542–563, 2013.
- [2] Seijas-Macías, Antonio and Oliveira, Amílcar. An approach to distribution of the product of two normal variables. *Discussiones Mathematicae Probability and Statistics*, 32(1-2):87–99, 2012.
- [3] Taylor, Benjamin, Davies, Tilman, Rowlingson, Barry, and Diggle, Peter. Bayesian inference and data augmentation schemes for spatial, spatiotemporal and multivariate log-Gaussian Cox processes in r. *Journal of Statistical Software*, 63:1–48, 2015.